Deterministic structural and fracture mechanics analyses of reactor pressure vessel for pressurized thermal shock

M.J. Jhung† and Y.W. Park‡

Korea Institute of Nuclear Safety, 19 Kusong-dong, Yusong-gu, Taejon 305-338, Korea

Abstract. The structural integrity of the reactor pressure vessel under pressurized thermal shock (PTS) is evaluated in this study. For given material properties and transient histories such as temperature and pressure, the stress distribution is found and stress intensity factors are obtained for a wide range of crack sizes. The stress intensity factors are compared with the fracture toughness to check if cracking is expected to occur during the transient. A round robin problem of the PTS during a small break loss of coolant transient has been analyzed as a part of the international comparative assessment study, and the evaluation results are discussed. The maximum allowable nil-ductility transition temperatures are determined for various crack sizes.

Key words: reactor vessel; pressurized thermal shock; stress intensity factor; fracture toughness; crack initiation; nil-ductility transition temperature.

1. Introduction

A nuclear reactor pressure vessel, which contains fuel assemblies and reactor vessel internals, is a very important structure because it keeps coolant of high temperature and high pressure during normal operation. Therefore, it is designed and manufactured according to strict regulations and studies on its structural integrity are under going actively (Mishima *et al.* 1994, Pennell 1993).

Since the Rancho Seco transient in 1978 (Stahlkopf 1984), a pressurized thermal shock has been designated as a severe safety issue. A pressurized thermal shock involves a transient in which severe overcooling causes a thermal shock to the vessel, while the pressure is either maintained or the system is repressurized during the transient. The thermal stress due to the rapid cooling of the vessel walls in combination with the pressure stress from either maintaining system pressure or repressurization of the system results in large tensile stresses which are maximum at the inside surface of the vessel. At the material temperature below its nil-ductility transition temperature, the combination of the pressure and thermal stresses could cause a decrease in fracture toughness and a relatively small crack propagation through the vessel wall. Therefore, it is necessary to evaluate a structural integrity of a reactor pressure vessel under a pressurized thermal shock event.

---

† Senior researcher
‡ Principal researcher

In this study, the fracture mechanics methodology for the pressurized thermal shock is introduced and a calculation routine for the PTS evaluation of the pressure vessel is developed. For given material properties, transient history such as temperature and pressure, and a postulated flaw, the stress distribution on the vessel wall is calculated and then stress intensity factors are obtained for various crack sizes. The stress intensity factors are compared with the material fracture toughness values to check the possibilities of the crack growth during the transient.

Using an analysis routine developed, a round robin problem of PTS during a small break loss of coolant transient has been analyzed as a part of the international comparative assessment study. The maximum allowable nil-ductility transition temperatures are determined for various crack sizes.

2. Calculation of temperature and stress distributions

2.1. Temperature distribution

Considering a very long cylindrical vessel with uniform fluid temperature, the temperature distribution in the vessel wall $T(r, t)$ is assumed to be governed by the ordinary differential equation (Ozisik 1980)

$$\rho c T_t - k\left(\frac{1}{r}T_r + T_{rr}\right) = 0 \tag{1}$$

subject to initial condition and boundary conditions

$$T(r, 0) = T_0$$
$$T_r(r_0, t) = 0$$
$$-kT_r(r_i, t) = h\left[T_c(t) - T(r_i, t)\right] \tag{2}$$

where T_0 is the initial coolant temperature, T_c the coolant temperature, k the heat conductivity of the material, h the heat transfer coefficient between the coolant and vessel material, ρ the material density, c the material specific heat, r_0 the outer radius, r_i the inner radius and t the time. Subscripts r and t represent the differentiation with respect to radial coordinate and time, respectively.

The finite difference equations for N radial points, at distance Δr apart, across the cross section of the vessel are (Myers 1971)

for $n=1$;

$$T_1^{t+\Delta t} = \left[1 - \frac{\Delta t \cdot k}{\rho c (\Delta r)^2}\left(1 + \frac{\Delta r}{r_1}\right) - \frac{\Delta t \cdot h}{\rho c (\Delta r)}\right] T_1^t + \frac{\Delta t \cdot k}{\rho c (\Delta r)^2}\left[\left(1 + \frac{\Delta r}{r_1}\right) T_2^t + \frac{\Delta t \cdot h}{k} T_c^t\right] \tag{3a}$$

for $1 < n < N$;

$$T_n^{t+\Delta t} = \left[1 + \frac{\Delta t \cdot k}{\rho c (\Delta r)^2}\left(2 + \frac{\Delta r}{r_n}\right)\right] T_n^t + \frac{\Delta t \cdot k}{\rho c (\Delta r)^2}\left[\left(1 + \frac{\Delta r}{r_n}\right) T_{n+1}^t + T_{n-1}^t\right] \tag{3b}$$

and for $n = N$;

$$T_n^{t+\Delta t} = \left[1 - \frac{\Delta t \cdot k}{\rho c (\Delta r)^2}\right] T_N^t + \frac{\Delta t \cdot k}{\rho c (\Delta r)^2} T_{N-1}^t \tag{3c}$$

For stability in the finite difference calculation, we must choose Δt for a given Δr that both

$$\frac{\Delta t \cdot k}{\rho c (\Delta r)^2} \left(2 + \frac{\Delta r}{r_1}\right) \leq 1 \quad \text{and} \quad \frac{\Delta t \cdot k}{\rho c (\Delta r)^2} \left(1 + \frac{\Delta r}{r_1}\right) + \frac{\Delta t \cdot h}{\rho c (\Delta r)} \leq 1 \tag{4}$$

are satisfied (Myers 1971).

2.2. Stress distribution

The thermal stress distribution is calculated using the results by (Timoshenko and Goodier 1970, Harvey 1960)

$$\sigma_{T, hoop}(r, t) = \frac{\beta E}{1 - \nu} \left[\frac{1}{r^2} \int_{r_i}^{r} T(r, t) \, r dr - T(r, t) + \frac{1}{r^2} \frac{r^2 + r_i^2}{r_o^2 - r_i^2} \int_{r_i}^{r_o} T(r, t) \, r dr \right] \tag{5}$$

$$\sigma_{T, axial}(r, t) = \frac{\beta E}{1 - \nu} \left[\frac{2}{r_o^2 - r_i^2} \int_{r_i}^{o} T(r, t) \, r dr - T(r, t) \right] \tag{6}$$

where E(ksi) is Young's modulus, β(ft/ft °F) the coefficient of thermal expansion, and ν Poisson's ratio. Poisson's ratio is taken to be constant while β and E are evaluated as a function of the average temperature T_{avg} across the vessel as follows:

$$T_{avg} = \frac{2}{r_o^2 - r_i^2} \int_{r_i}^{r_o} T(r, t) \, r dr \tag{7}$$

The stresses $\sigma_p(r, t)$ due to internal pressure p are calculated using the following equations (Timoshenko and Goodier 1970, Harvey 1960):

$$\sigma_{p, hoop}(r, t) = p(t) \frac{r_i^2}{r_o^2 - r_i^2} \times \frac{r_o^2 + r^2}{r^2} \tag{8}$$

$$\sigma_{p, axial}(r, t) = \frac{1}{2} p(t) \frac{r}{r_o - r_i} \tag{9}$$

where r_o is the outer radius and r_i the inner radius.

3. Fracture mechanics analysis

3.1. Stress intensity factor

Stress intensity factor for the flaw is calculated from the membrane and bending stresses determined from stress analysis at the flaw location as shown in Fig. 1 using the following equation (ASME 1995b):
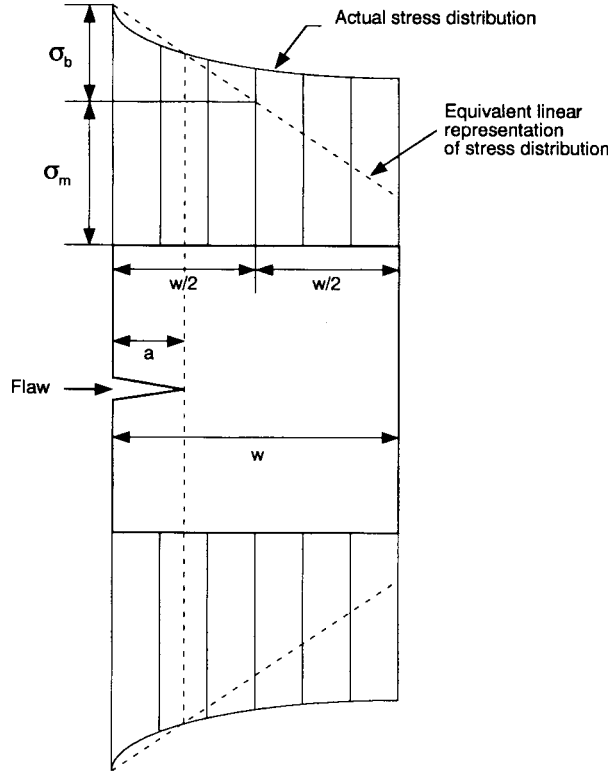
M.J. Jhung and Y.W. Park

Fig. 1 Membrane and bending stress classification

$$K_I = \sqrt{\pi \frac{a}{Q}} \, (M_m \, \sigma_m + M_b \, \sigma_b) \tag{10}$$

where σ_m is the membrane stress (ksi), σ_b the bending stress (ksi), M_m the correction factor for membrane stress, M_b the correction factor for bending stress, a the flaw depth for inner surface flaw and Q the flaw shape factor. The stresses σ_m and σ_b are determined from Fig. A 3200-1 of ASME Code Section XI, Appendix A (ASME 1995b), M_m and M_b from Fig. A 3300-2~5, and Q from Fig. A 3300-1.

3.2. Fracture toughness

The fracture toughness of the material is defined by two properties K_{IA} and K_{IC}, which represent critical values of the stress intensity factor. K_{IA} is based on the lower bound of crack arrest critical K_I values measured as a function of temperature. K_{IC} is based on the lower bound of static initiation critical K_I values measured as a function of temperature. Lower bound K_{IA} and K_{IC}, versus temperature curves from tests of SA-533 Grade B Class 1, SA-508 Class 2, and SA-508 Class 3 steel are provided in Fig. A 4200-1 of ASME Code Section XI, Appendix A (ASME 1995b) and can be represented as:

$$K_{IC} = 33.2 + 2.806 e^{0.020(T - RT_{NDT} + 100)} \tag{11}$$

$$K_{IA} = 26.8 + 1.233 e^{0.0145(T - RT_{NDT} + 160)} \tag{12}$$

where RT_{NDT} is the reference temperature of nil-ductility transition which is given by the following expression:

$$RT_{NDT} = RT_{NDT0} + \Delta RT_{NDT} \tag{13}$$

The initial RT_{NDT}, RT_{NDT0}, is the reference temperature for the unirradiated material as defined in Paragraph NB-2331 of ASME Code Section III (ASME 1995a) and ΔRT_{NDT} is the mean value of the adjustment in reference temperature caused by irradiation and is calculated as follows:

$$\Delta RT_{NDT} = CF \times f^{0.28 - 0.101 \log f} \tag{14}$$

where CF (°F) is the chemistry factor, a function of copper and nickel content, determined from Regulatory Guide 1.99, Rev.2 (USNRC 1988). The neutron fluence in the vessel wall, $f(10^{19}$ n/cm^2, E > 1 MeV), is determined as follows:

$$f = f_{surf} \, e^{-0.24a} \tag{15}$$

where f_{surf} (10^{19} n/cm^2, E > 1 MeV) represents the neutron fluence at the wetted inner surface of the vessel at the location of the postulated defect and a (in inches) is the depth into the vessel wall measured from the vessel inner surface.

4. Evaluation method

4.1. Critical crack depth

Using the profiles of the stress and temperature, stress intensity factors are calculated for various penetration depths. The crack arrest K_{IA} and crack initiation K_{IC} fracture toughness profiles are also determined using the irradiated fracture toughness data. For each time during the transient, the variations of K_I, K_{IC} and K_{IA} through the thickness are determined as shown in Fig. 2. The crack penetration at which the calculated stress intensity factor exceeds K_{IC} profile corresponds to the critical size for crack initiation (a_c), and the penetration at which the stress intensity factor goes below the K_{IA} curve corresponds to the critical size for crack arrest (a_a). Graphs of a_c and a_a versus time, called a critical crack depth diagram, are then prepared as shown in Fig. 3. A critical crack depth diagram consists of curves for initiation $(K_I = K_{IC})$, arrest $(K_I = K_{IA})$, and upper shelf toughness $(K_I = 200$ ksi$\sqrt{in}$). The behavior of a crack initiation and arrest can be predicted from this diagram for the assumed crack with a postulated transient. If there is a crack with $a/w = 0.20$, it is initiated twice following the dotted line resulting in through-wall propagation. In Fig. 3, (a_1, t_1) is a crack size and time when a first initiation occurs and $a_2 \sim a_3$ is the range of the crack sizes which can be initiated during a transient. If a crack is so small or large and is beyond this range, it is not initiated. The smallest value of a_c, a_2, is used for comparison with acceptance criteria.

4.2. Warm prestressing

Several studies (McGowan 1979, Curry 1983) have shown that the fracture toughness can be significantly increased at low temperatures if the material is prestressed at a higher temperature. A conservative method is formulated to use this warm prestressing (WPS) effect in the fracture mechanics of pressure vessels under thermal shock. This method uses the basic premise that a crack will not initiate when the stress intensity factor is dropping with time or constant, whether
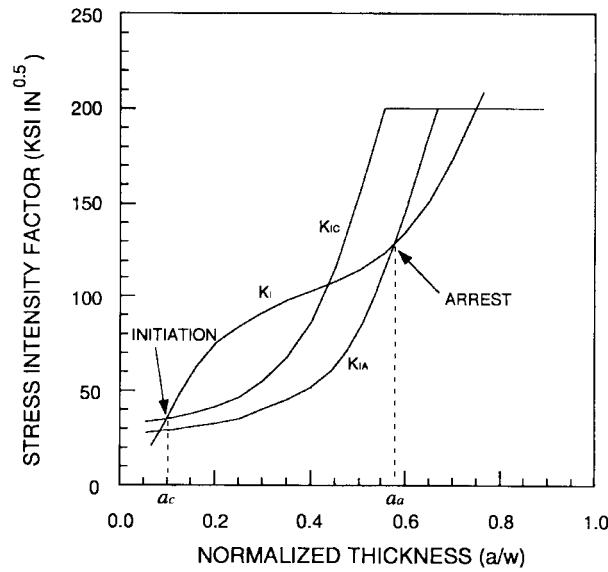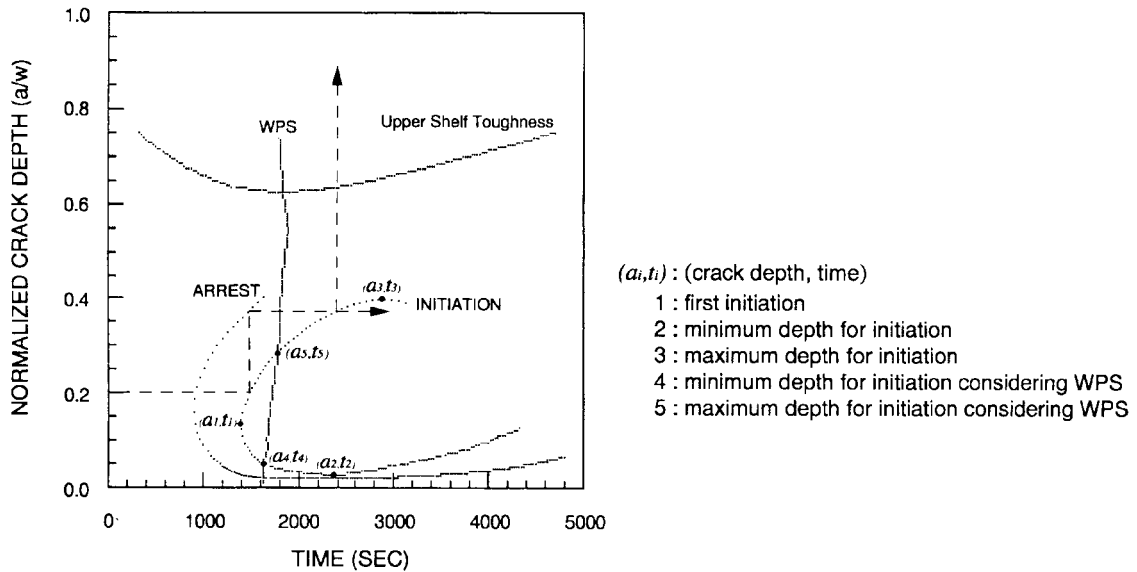
Fig. 2 Determination of critical flaw sizes

Fig. 3 Typical critical crack depth diagram

or not the temperature is dropping.

According to the classical linear elastic fracture mechanics, flaws will begin to initiate when K_I exceeds K_{IC}. However, according to the conservative warm prestressing principle, K_I must exceed K_{IC} before the maximum K_I occurs, for initiation to take place; otherwise initiation cannot occur when K_I is dropping with time. For each flaw depth, the time (θ_{max}) for the peak K_I to occur is determined. The variation of θ_{max} with crack depth is then plotted on the same graph as a_c and a_a versus time. Therefore warm prestressing curve ($dK_I/dt = 0$) is also included in the critical crack depth diagram. For a given flaw depth, if the θ_{max} curve is crossed before a_c curve, no initiation
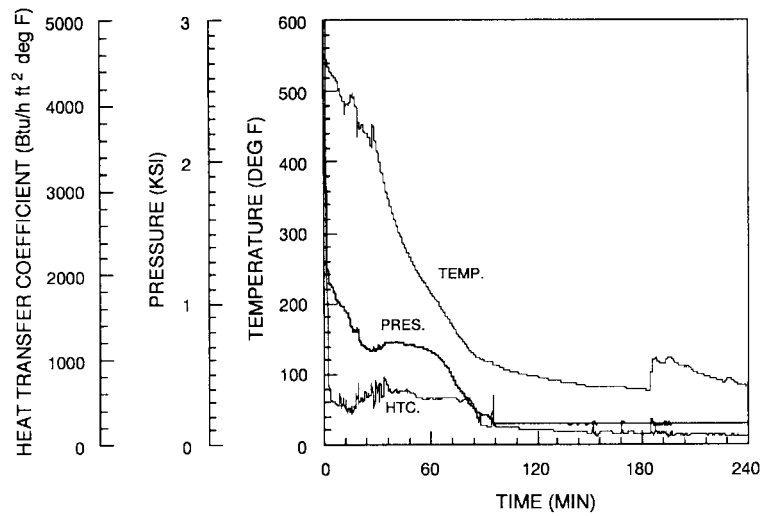
Fig. 4 Pressure, temperature and heat transfer coefficient histories

Table 1 Postulated cracks

Number	Location	Direction	Shape	Aspect Ratio (a/l)	Depth $(a,$ inch)	Eccentricity $(e,$ inch)
C1	surface	circumferential	360°	0	0.6299	
C2	surface	circumferential	semi-elliptical	1/6	0.6299	
C3	surface	axial	semi-elliptical	1/6	0.6299	
C4	subsurface	circumferential	elliptical	1/12	0.1969	4.4685
C5	subsurface	axial	elliptical	1/12	0.1969	4.4685

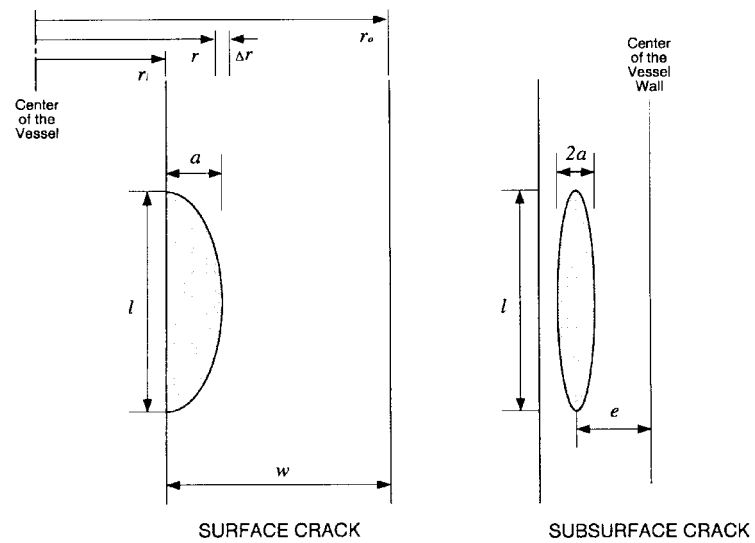

Fig. 5 Postulated cracks

will occur because of warm prestressing. In Fig. 3, a crack (a/w=0.20) is initiated once, arrested at about a/w=0.375 and is not initiated again. Considering a warm prestressing effect, the intersections of the θ_{max} curve and a_c curve define the range of flaw sizes that would initiate. In Fig. 3, a_4~a_5 is the range of the crack sizes which can be initiated during a postulated transient. The minimum flaw (a_4) that would initiate is determined by the lowest intersection of the θ_{max} and the a_c curves; the maximum flaw (a_5) that would initiate is determined by the highest intersection of the θ_{max} and the a_c curves.

4.3. Determination of maximum allowable RT_{NDT}

If a crack with a specific size and a shape is given, it is necessary to check whether it is initiated or not during the PTS transient. In this case the deepest point of a crack should be investigated for a possible initiation. The temperature and stress intensity factor histories at crack tip are calculated. Also the fracture toughness K_{IC} is determined using Eq. (11) for the variations of RT_{NDT} which is assumed arbitrarily. The maximum allowable RT_{NDT} is the low bound found by tangent criteria when K_{IC} curve meets K_I curve tangentially. In the same way, the upper bound of allowable RT_{NDT} is determined when K_{IC} curve intersects a maximum point of K_I curve, which is considering a warm prestressing effect and is called maximum criteria. Even though the RT_{NDT} of the material is higher than the low bound determined by tangent criteria, the crack will not be initiated due to warm prestressing effect if it is lower than the upper bound. Therefore the range of allowable RT_{NDT} is determined by two criteria, tangent criteria and maximum criteria depending on the warm prestressing effect.

5. Round Robin analysis for OECD/NEA PWG-3

5.1. Problem definition

The reactor pressure vessel is loaded by emergency cooling transients due to assumed leaks. Transient is due to a small break loss of coolant accident. The primary pressure and the averaged fluid temperatures as well as heat transfer coefficients in the downcomer are presented in Fig. 4. For this transient axial symmetric loading conditions with no change in axial position are assumed. The postulated flaws are surface and subsurface cracks with various shapes as shown in Table 1 and Fig. 5. This is one of round robin problems defined by Principal Working Group No. 3 of the Organization for Economic Cooperation and Development (OECD)/Nuclear Energy Agency (NEA) Committee for the International Comparative Assessment Study on the Reactor Pressure Vessel Pressurized Thermal Shock (Sievers 1996).

The temperature and stress distribution in the vessel wall is to be shown according to the given material properties (Table 2) and the postulated transient. Also the crack loading of the postulated cracks will be analyzed along the crack front. For each crack a fracture assessment concerning crack initiation is performed in the sense that a maximum allowable RT_{NDT} is determined.

To investigate the influence of residual stress, two distributions as shown in Fig. 6 are considered separately and together (Sievers 1996). Distribution 1 is related to residual stresses in circumferential weld due to the welding process and is characterized by the formula:

$$y(x) = y_{max} \cos\left(2\pi \cdot \frac{x}{x_{max}}\right) \qquad (16)$$

Table 2 Vessel parameters for the analysis

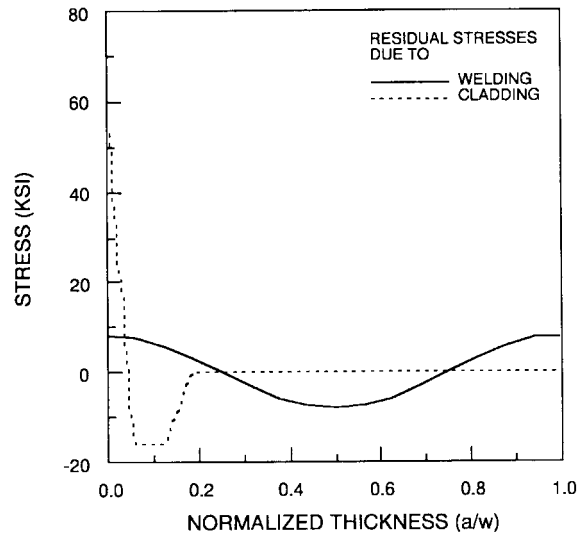|	
vessel thickness	9.806 inches
vessel inner radius	98.425 inches
material	SA 508 Class 3
Cu content	0.30 weight %
Ni content	0.75 weight %
initial RT_{NDT}	20°F

Fig. 6 Residual stress distributions

where x: radial coordinate measured from inner surface of the weld (> 0), x_{max}: wall thickness, and $y_{max} = 8.1$ ksi. Distribution 2 is related to the residual stresses due to the cladding process after heat treatment.

Also, various aspect ratios, i.e., $a/l = 1/6$, $1/4$, $1/2$ for surface crack and $a/l = 1/12$, $1/8$, $1/4$ for sub-surface crack, are considered to investigate the influence of them.

5.2. Results and discussion

The temperature distribution in the vessel wall is calculated from the coolant temperature variations during the transient. Fig. 7 shows the temperature histories of the vessel wall at $a/w = 0.065$, 0.5, 0.75 and 1.0 locations. Fig. 8 shows the temperature distributions in the vessel wall. The hoop and axial stress distributions versus time are shown in Fig. 9.

Using the Eqs. (10), (11) and (12), the K_I, K_{IC} and K_{IA} variations through the thickness are determined for each time step during the transient. Their distributions at time = 3000 seconds are shown in Fig. 10 for 360° circumferential crack (C1). There are two regions where K_I exceeds K_{IC} : $a/w = 0.0215$ to 0.3300 (transient behavior), and $a/w = 0.4351$ (upper shelf behavior). There is also an arrest point $a/w = 0.0138$. A summary of all initiation and arrest points for all times is shown in the critical crack depth diagram as shown in Fig. 11. For the fluence of $f = 3.5$ (Fig. 11), the critical crack depth, i.e., minimum crack size for initiation is $a/w = 0.0131$.
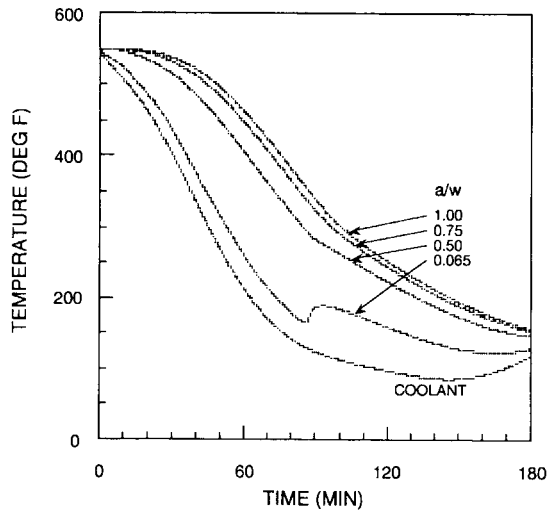
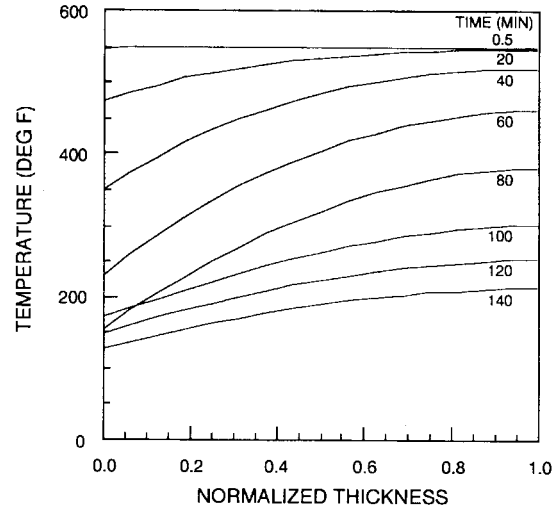Fig. 7 Temperature histories of the vessel wall and coolant

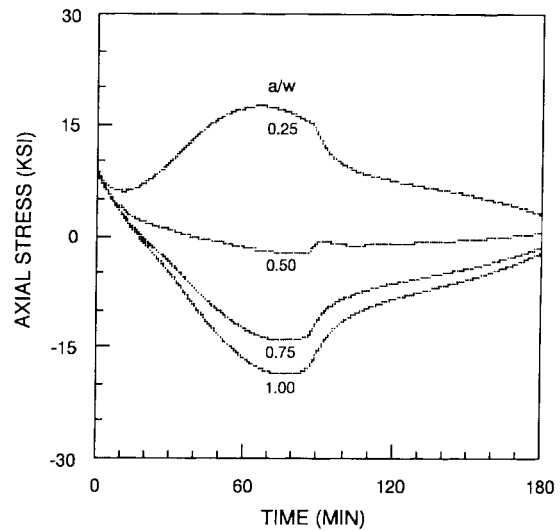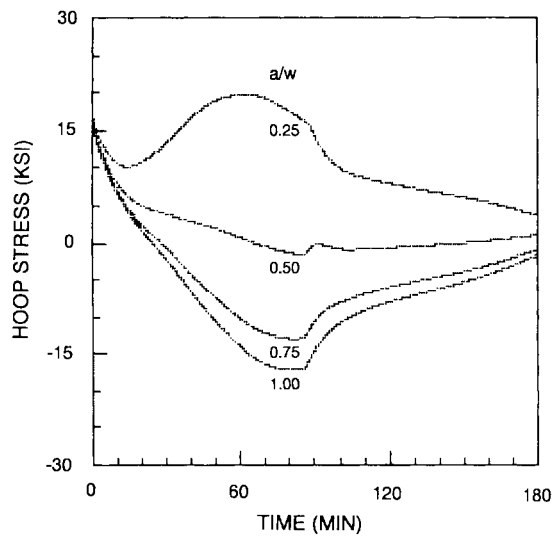Fig. 8 Temperature distributions through the vessel wall

Fig. 9 Hoop and axial stress histories of the vessel wall

In the warm prestress analysis, the K_I variation with time is determined for each crack depth considered and is shown in Fig. 12. For the 360° circumferential crack, the maximum K_I value 72.23 ksi$\sqrt{in}$ occurs at 3885 ($\theta_{max} = 3885$) seconds for $a/w = 0.065$, and they decrease from that point. This K_I value is well comparable with 72.8 ksi$\sqrt{in}$ computed by the finite element method (Sievers 1997). Even though K_I value exceeds K_{IC} for this crack depth, there is no initiation beyond this point θ_{max} because K_I is falling. A summary of θ_{max} for each crack depth is also included in the critical crack depth diagram (Fig. 11).

To get a maximum allowable RT_{NDT} for crack not to be initiated, the K_I and K_{IC} values at the deepest point are compared as shown in Figs. 13 through 15 for 360° circumferential, semielliptical circumferential and axial surface cracks with $a/l = 1/6$, respectively. The low and
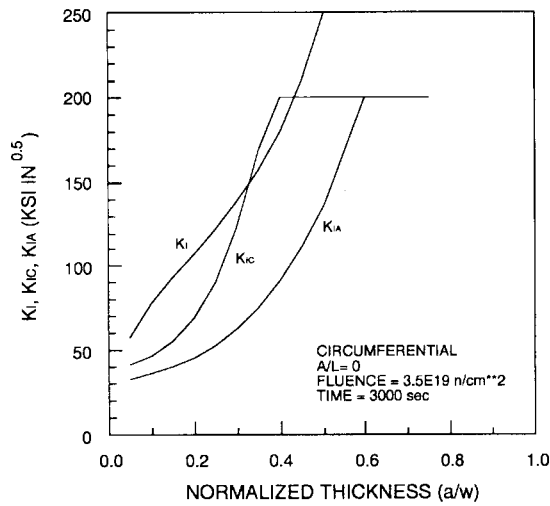
Fig. 10 Determination of critical crack sizes for circumferential crack
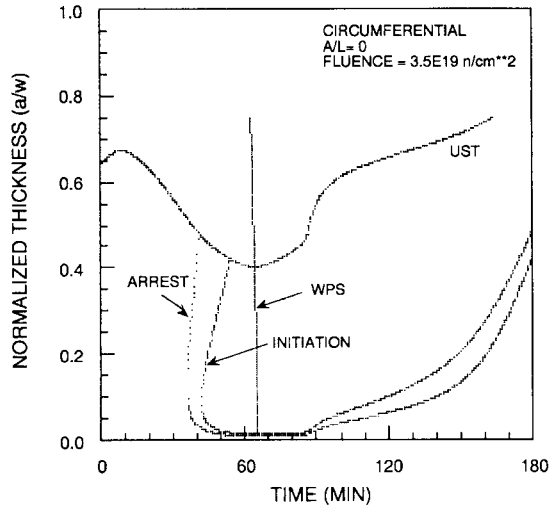

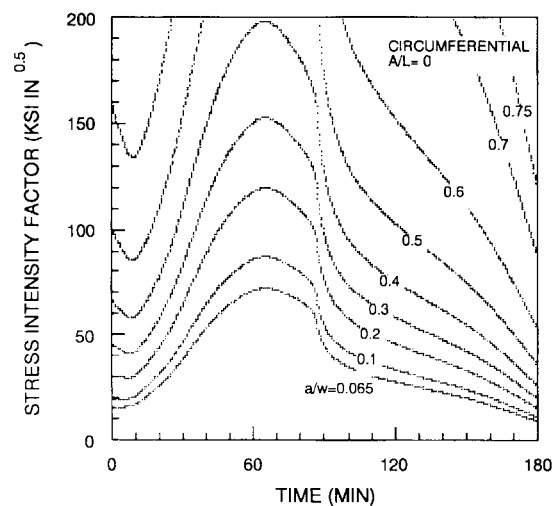Fig. 11 Critical crack depth diagram for circumferential crack

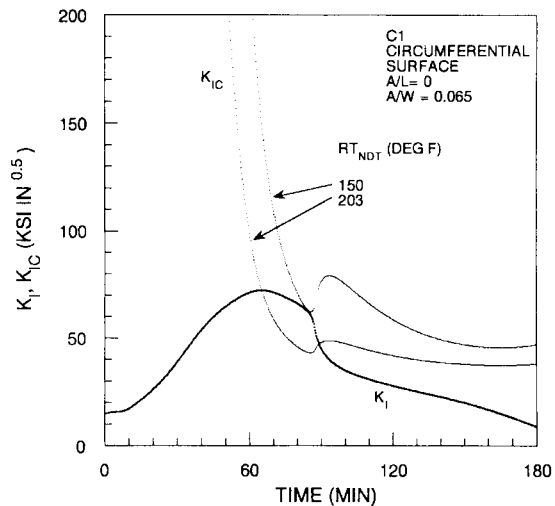Fig. 12 Stress intensity factor histories

Fig. 13 Determination of allowable RT_{NDT} for circumferential crack $(a/l = 0)$

upper bounds of RT_{NDT} for crack to be initiated are determined and summarized in Table 3. The maximum allowable RT_{NDT}s are 150, 186 and 178°F for 360° circumferential surface crack, semielliptical circumferential crack and axial surface crack with $a/l = 1/6$, respectively. For the subsurface cracks, the stress intensity factor versus crack tip temperature is given for the deepest crack front point as shown in Figs. 16 and 17 for circumferential and axial cracks, respectively. The load curve is well below the fracture toughness curve for the circumferential subsurface crack (C4). At the deepest point the maximum load of 31.33 ksi√$\overline{in}$ is reached at time of 65 minutes and temperature of 234°F. For the axial subsurface crack (C5) two different values of allowable RT_{NDT} are obtained as 397°F and 392°F according to the maximum and tangent criteria, respectively. If surveillance test indicates higher value of RT_{NDT} at the end of life, there is a
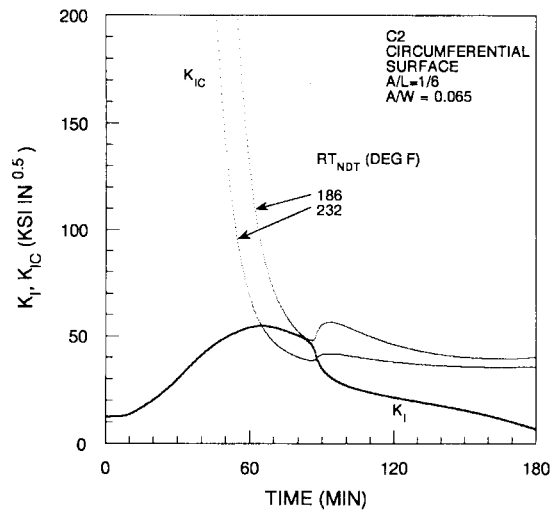
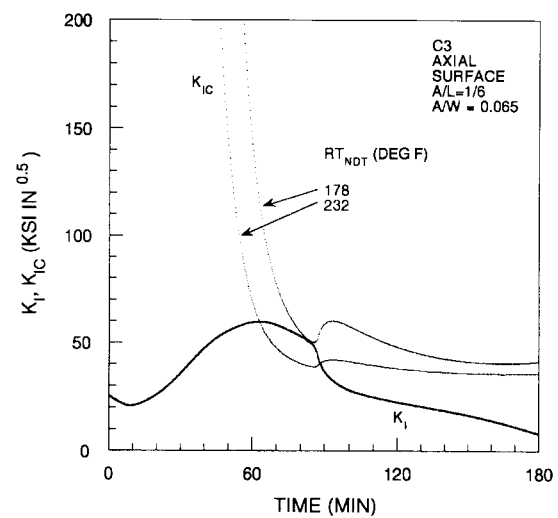Fig. 14 Determination of allowable RT_{NDT} for semielliptical circumferential crack ($a/l = 1/6$)

Fig. 15 Determination of allowable RT_{NDT} for semielliptical axial crack ($a/l = 1/6$)

Table 3 Maximum stress intensity factors and allowable RT_{NDT}s at the deepest point

| crack number | residual stress distribution[1] | maximum K_I | | maximum allowable RT_{NDT} | | | |
| | | value (ksi√in) | time (min) | maximum criteria | | tangent criteria | |
				value	time	value	time
C1	none	72.2	64.8	203	64.8	150	84.1
	1	91.9	64.8	183	64.8	126	84.1
	2	111.5	64.8	168	64.8	110	84.3
	1+2	142.0	64.8	152	64.8	93	84.5
C2	none	54.7	64.8	232	64.8	186	83.2
	1	67.1	64.8	211	64.8	156	84.0
	2	80.9	65.0	194	65.0	136	84.3
	1+2	98.3	64.8	179	64.8	119	84.5
C3	none	59.7	63.0	232	63.0	178	82.3
	1	72.7	63.0	211	63.0	151	83.8
	2	87.2	63.0	194	63.0	133	83.7
	1+2	106.1	62.8	179	62.8	116	84.5
C4	none	31.3	65.0	> 600	-	> 600	-
	1	39.3	65.0	295	65.0	268	76.3
	2	47.5	64.8	253	64.8	209	82.5
	1+2	59.4	64.8	223	64.8	171	83.7
C5	none	34.2	63.0	397	63.0	392	65.0
	1	42.6	63.0	283	63.0	248	77.8
	2	51.3	63.0	250	63.0	200	82.3
	1+2	64.3	63.0	221	63.0	166	83.6

[1]Include residual stresses due to
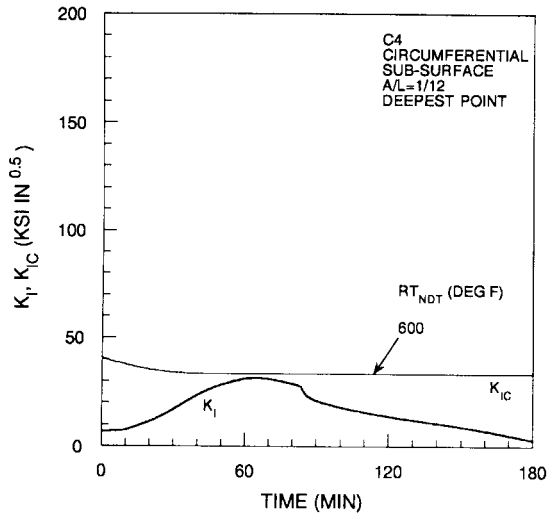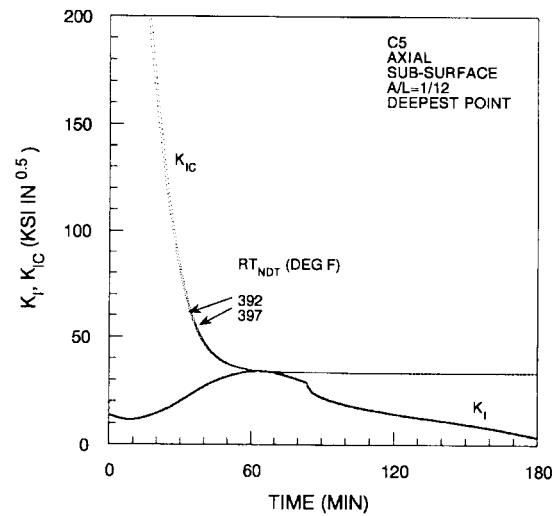1: circumferential welding, 2: cladding after heat treatment

Fig. 16 Determination of allowable RT_{NDT} for elliptical circumferential subsurface crack

Fig. 17 Determination of allowable RT_{NDT} for elliptical axial subsurface crack

Table 4. Maximum allowable RT_{NDT}s with various aspect ratios

crack	aspect ratio (a/l)	criteria (deg F)	
		maximum	tangent
surface	0	203	150
circumferential	1/6	232	186
	1/4	249	206
	1/2	339	329
surface	0	203	145
axial	1/6	232	178
	1/4	246	196
	1/2	310	285
sub-surface	0	> 600	> 600
circumferential	1/12	> 600	> 600
	1/8	> 600	> 600
	1/4	> 600	> 600
sub-surface	0	348	336
axial	1/12	397	392
	1/8	> 600	> 600
	1/4	> 600	> 600

possibility of through-wall propagation in the assumed crack.

The maximum allowable RT_{NDT}s for the case with residual stress included are shown in Table 3. The effect of residual stress due to cladding is more severe than that due to welding. For the surface cracks the allowable RT_{NDT}s considering warm prestressing effect are the same irrespective of the crack direction, but there is a little difference between circumferential and axial cracks by tangent criteria.

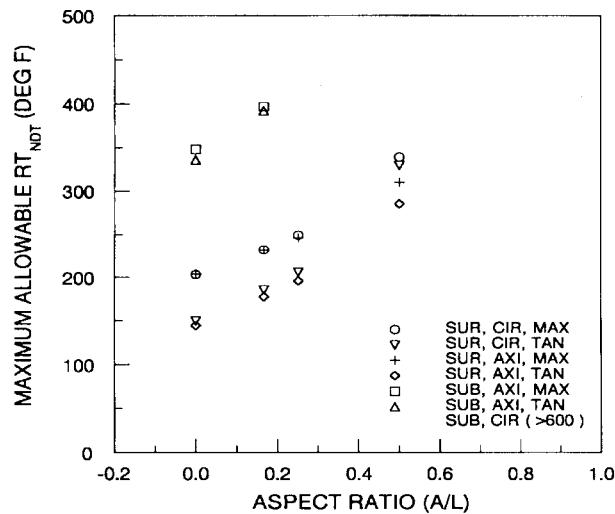The maximum allowable RT_{NDT}s for various aspect ratios are shown in Table 4 and Fig. 18,

Fig. 18 Maximum allowable RT_{NDT}s with respect to aspect ratios

from which allowables are found to be increased linearly with repect to aspect ratio.

6. Conclusions

The structural integrity of the reactor pressure vessel under pressurized thermal shock is evaluated. For given material properties and transient histories such as temperature and pressure, the stress distribution is calculated and stress intensity factors are obtained for various crack sizes. The stress intensity factors are compared with the fracture toughness to check if cracking is expected to occur during the transient.

A round robin problem of PTS during a small break loss of coolant transient has been analyzed as a part of the international comparative assessment study. The maximum allowable value of RT_{NDT} is 150°F for a 360° circumferential surface crack with $a/w = 0.065$, and about 180°F for axial and circumferential surface cracks with $a/l = 1/6$. Considering warm prestressing effect, these values are over 200°F. The allowable for the subsurface crack with $a/l = 1/12$ is over 390°F and is therefore found to be insignificant for the transient considered. The allowables with residual stress due to welding and cladding are lower than those of stress free condition by about 30°F. If RT_{NDT} at the end of life is anticipated to exceed the allowables by surveillance test, actions should be taken to prevent the postulated crack from being initiated due to a PTS transient.

Structural integrity of the pressure vessel in view of PTS may be evaluated using the analysis routine developed in this study. Especially for the life extension of the old plant, this study can be used.

References

ASME (1995a), "Rules for construction of nuclear power plant components", *ASME Boiler and Pressure Vessel Code*, Section III.

ASME (1995b), "Rules for inservice inspection of nuclear power plant components", ASME Boiler and Pressure Vessel Code, Section XI.

Curry, D.A. (1983), "A model for predicting the influence of warm pre-stressing and strain aging on the cleavage fracture toughness of ferritic steels", *International Journal of Fracture*, **22**, 145-159.

Harvey, J.F. (1960), *Theory and Design of Modern Pressure Vessels*, 2nd ed., Van Nostrand Reinhold Co., New Jersey.

McGowan, J.J. (1979), "Application of warm prestressing effects to fracture mechanics analyses of nuclear reactor vessels during severe thermal shock", *Nuclear Engineering and Design*, **51**, 431-444.

Mishima, Y., et al. (1994), "PTS integrity study in Japan", *International Journal of Pressure Vessels and Piping*, **58**, 91-101.

Myers, M.N. (1971), *Analytical Method in Conduction Heat Transfer*, McGraw-Hill, New York.

Ozisik, M.N. (1980), *Heat Conduction*, John Wiley & Sons.

Pennell, W.E. (1993), "Heavy-section steel technology program overview", *Nuclear Engineering and Design*, **142**, 117-135.

Sievers, J. (1996), "Reactor pressure vessel pressurized thermal shock international comparative assessment study", OECD/NEA PWG-3, December 23.

Sievers, J. (1997), "The interim workshop on RPV PTS ICAS", OECD/NEA PWG-3, June 2.

Stahlkopf, K.E. (1984), "Pressure vessel integrity under pressurized thermal shock conditions", *Nuclear Engineering and Design*, **80**, 171-180.

Timoshenko, S.P. and Goodier, J.M. (1970), *Theory of Elasticity*, 3rd ed., McGraw-Hill, New York.

USNRC (1988), "Radiation embrittlement of reactor vessel materials", Regulatory Guide 1.99, Rev.2, US Nuclear Regulatory Commission, May.

Appendix - Material properties

The linear regression analysis of the tabular values of the ASME Code Section III (ASME 1995a) results in the following expressions for the material properties such as the thermal conductivity k (btu/hr-ft-°F), the thermal diffusivity α (ft^2/hr), Young's modulus E (ksi) and the coefficient of thermal expansion β (ft/ft °F) for SA508 Class 3 and SA533B Class 1.

$$E = \left(27.968 - .53395\frac{T}{10^2} + .65784\frac{T^2}{10^5} - .92201\frac{T^3}{10^8} \right) \times 10^3 \qquad \text{(A-1)}$$

SA508 Class 3 :

$$k = 21.309 + .88517\frac{T}{10^2} - .19641\frac{T^2}{10^4} + .91496\frac{T^3}{10^8} \qquad \text{(A-2)}$$

$$\alpha = .43040 - .14836\frac{T}{10^3} - .45642\frac{T^2}{10^7} + .16109\frac{T^3}{10^{11}} \qquad \text{(A-3)}$$

$$\beta = 10^{-6} \times \left(6.2996 + .18464\frac{T}{10^2} + .32482\frac{T^2}{10^6} - .44579\frac{T^3}{10^9} \right) \qquad \text{(A-4)}$$

SA533B Class 1 :

$$k = 21.303 + .16033\frac{T}{10^1} - .29469\frac{T^2}{10^4} + .12344\frac{T^3}{10^7} \qquad \text{(A-5)}$$

$$\alpha = .42549 + .68456\frac{T}{10^4} - .51640\frac{T^2}{10^6} + .28578\frac{T^3}{10^9} \tag{A-6}$$

$$\beta = 10^{-6} \times \left(6.8420 + .23285\frac{T}{10^2} - .14897\frac{T^2}{10^5} + .58824\frac{T^3}{10^9} \right) \tag{A-7}$$

where T is °F.